Nonlinear dynamics of forced wavepackets in turbulent jets

Igor A. Maia* and Peter Jordan†
Institut Pprime-CNRS-Université de Poitiers-ENSMA. Poitiers, France.

Liam Heidt‡ and Tim Colonius§
California Institute of Technology, Pasadena, CA, USA

Akhil Nekkanti¶ and Oliver T. Schmidt‖
University of California San Diego, La Jolla, CA, USA

We study the dynamics of harmonically-forced jets under different forcing amplitudes covering linear and nonlinear response regimes. Using a combination of Particle Image Velocimetry (PIV) measurements, Spectral Proper Orthogonal Decomposition (SPOD) and Bispectral Mode Decomposition (BMD), we educe coherent structures on the different forcing regimes and analyse how strong nonlinear interactions affect their dynamics. The forced jets provide a simplified scenario where energy exchange between frequencies can be traced back to a few prominent triadic interactions. These are identified through the mode bispectrum and the associated BMD modes are found to be in good agreement with the most energetic structures computed through SPOD. The mode bispectrum also provides insight into the relative importance of linear and nonlinear mechanisms, with respect to the mean of the forced jet, in determining the amplitudes of velocity fluctuations at the forcing frequency and its harmonics. Unforced jets have a broad signature in the bispectrum, reflecting the broadband nature of nonlinear energy exchange in the unforced jets.

I. Nomenclature

Re	=	Reynolds number
U_j	=	Jet exit velocity
c_∞	=	Sound speed
Ma	=	Mach number
St	=	Strouhal number
D	=	Jet diameter
x	=	Streamwise coordinate
r	=	Transverse coordinate
θ	=	Shear-layer momentum thickness
$\mathbf{q}$	=	State vector
$\hat{\mathbf{S}}_{\omega_k}$	=	Cross-spectral density matrix
$\mathbf{\Psi}_{\omega_k}$	=	SPOD eigenmodes

*Post-Doctoral Research Fellow, Département Fluides Thermique et Combustion, Institut Pprime-CNRS-Université de Poitiers-ENSMA. Poitiers, France.

†Directeur de Recherche, Département Fluides Thermique et Combustion, Institut Pprime-CNRS-Université de Poitiers-ENSMA. Poitiers, France.

‡PhD Student, Division and Engineering and Applied Science, California Institute of Technology, Pasadena, CA, USA

§Frank and Ora Lee Marble Professor of Mechanical Engineering, Division and Engineering and Applied Science, California Institute of Technology, Pasadena, CA, USA

¶PhD Student, Department of Mechanical and Aerospace Engineering, University of California San Diego, La Jolla, CA, USA

‖Assistant Professor, Department of Mechanical and Aerospace Engineering, University of California San Diego, La Jolla, CA, USA

λ_{ω_k}	=	SPOD eigenvalues
$\mathbf{W}$	=	Quadrature weights
$b(f_k, f_l)$	=	Integral bispectrum measure for a pair of frequencies f_k and f_l
ϕ_{k+l}	=	Bispectral Modes
$\phi_{k\circ l}$	=	Cross-frequency modes
$\hat{\mathbf{Q}}_{\omega_k}$	=	Vector of ensemble flow realisations
$\mathbf{a}_1$	=	BMD expansion coefficients
$\mathbf{B}$	=	Bispectral density matrix
λ_1	=	Numerical radius of $\mathbf{B}$

II. Introduction

Many studies on harmonically-forced jets have been conducted in the past, for a wide range of forcing frequencies. The goal of these experiments has often been to study the dynamics of instability waves, also referred to as wavepackets. The forcing provides a phase-locking mechanism that raises those structures above the level of background turbulence, making their eduction easier. For sufficiently low levels of forcing amplitudes, the jet response has been found to be linear, and the dynamics of the forced wavapackets are essentially the same as those from unforced jets [1, 2]. This hypothesis has formed the basis for many early studies that aimed at inferring the dynamics of wavepackets and their associated sound field in unforced jets from their forced counterparts [3–9].

More recently, the understanding and modelling of wavepacket dynamics in unforced jets has made meaningful strides, supported by the advancement in measurement techniques, notably Particle Image Velocimetry (PIV) [10, 11], advanced signal processing tools such as Spectral Proper Orthogonal Decomposition (SPOD) [12] and modelling tools, such as the Parabolised Stability Equations (PSE) [10, 13, 14] and Resolvent Analysis [15–17].

These studies have shown that many important features of jet dynamics and sound radiation can be successfully explained by linear models. However, these models also possess severe limitations due to the lack of nonlinear phenomena. In particular, the absence of information about nonlinear forcing term in the context of resolvent analysis prevents these models from predicting the amplitude of the wavepackets, or to fully understand the mechanisms by which they become spatially desynchronised when convected by the flow, leading to increased acoustic efficiency.

Even in most forced-jet studies, nonlinearity in the jet response with high-amplitude forcing is usually only lightly addressed. Nonlinear response to harmonic forcing has been reported to cause significant changes in broadband near-field turbulent fluctuations [18] and broadband far-field noise [19], but there is conflicting evidence between different studies as to what are the precise dynamics underpinning such phenomena, and under what upstream conditions [20]. An important issue is the the distinction between linear and nonlinear behaviour. A thorough characterisation of the onset of nonlinearity with increasing forcing amplitude and how it changes the dynamics of coherent structures has not often been done, with a few exceptions [21–23]. Even with a modern tool adapted to educe coherent structures, such as SPOD, distilling nonlinear mechanisms is not straightforward, as it cannot provide any information about the energy exchange across different frequencies.

Here we intend to address some of these issues through an association of experimental data, SPOD and Bispectral Mode Decomposition (BMD) [24], a novel technique design to educed flow structures issuing from triadic interactions. The database consists of PIV measurements of turbulent jets forced harmonically at different amplitudes, so as to explore linear and nonlinear response regimes. A database for an unforced jet is used as baseline. Our goal is to characterise the dynamics of coherent structures in the different regimes in order to gain insight into nonlinear mechanisms for future modelling work. Working with forced jets offers a simplified scenario for analysis, since the flow energy is dominated by interactions issuing from only a few triadic interactions, as opposed to the broadband character of the unforced jet.

The paper is organised as follows: in section §III we describe the experimental setup; in §IV we present the mathematical description of the tools used, i.e, SPOD and BMD; this is followed by the results of the analysis in §V and by concluding remarks in §VI.

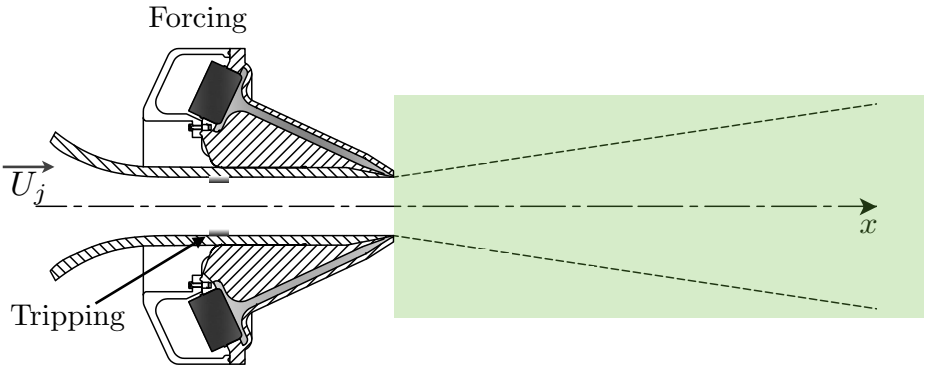

Fig. 1 Schematic of the experimental setup. Synthetic jets generated by loudspeakers force the jet at the nozzle lip. The green-shaded area corresponds to the PIV measurement plane, which spans the region $-1.5 \leqslant r/D \leqslant 1.5$**,** $0 \leqslant x/D \leqslant 6$**.**

III. Experimental setup

The experiments were performed in a low-Mach-number facility at the Pprime Institute, in Poitiers, France. The jet Mach ($Ma = U_j/c_\infty$) and Reynolds ($Re = U_j D/\nu$) numbers are 0.05 and 5×10^4, respectively, with U_j the jet exit velocity, c_∞ the ambient speed of sound and ν the kinematic viscosity of the air. The nozzle diameter is 50mm. The jet is forced with axisymmetric disturbances generated by a system of eight loudspeakers positioned in a conical structure that fits the nozzle. The loudspeakers generated synthetic jets that exit through a 0.01D annular gap and force the main jet at the nozzle lip. Forcing amplitude modified by varying the tension applied to the loudspeaker system. It is the same setup used by Maia et al. [25].

PIV measurements were performed in a plane parallel to the jet axis defined by $-1.5 \leqslant r/D \leqslant 1.5$, $0 \leqslant x/D \leqslant 6$, where r and x are the radial and streamwise coordinates, respectively. The PIV system consisted of two Photron APS-RS cameras and a 527 nm 30mJ Continuum TERA PIV laser. The sampling frequency of the cameras was limited to 1.5kHz, and the measurement time was set to 2700 convective time units, with a convective time unit defined by D/U_J. Complementary hot-wire measurements were also carried out in a few positions of the measurement plane.

The measurements were performed in jets issuing from nozzles with both untripped and tripped boundary layers. The former produces a laminar boundary layer at the exit which agrees well with the Blasius profile; the latter, on the other hand, produces a fully-turbulent boundary layer. The tripping is achieved using a strip of carborundum particles placed 2.5D upstream of the nozzle exit. In the initially-laminar jet, transition to turbulence occurs approximately 0.5D downstream of the nozzle exit. Boundary layer profiles for the initially-laminar and turbulent jets are reported by Maia et al. [25].

Prior to the PIV campaign, a series of hot wire measurements was made in order to identify the different response regimes of jets forced at different amplitudes at frequencies corresponding to Strouhal numbers of $St = 0.3, 0.4, 0.5$. For that, the hot wire was arbitrarily placed in the jet centerline two diameters downstream of the nozzle exit. Figure 2 shows the response of the turbulent jet to harmonic forcing at $St = 0.4, 0.5$ as a function of the voltage applied to the forcing system. For sufficiently low forcing amplitudes, clear linear regime, delimited approximately by the vertical dashed lines, are seen for the three forcing frequencies. Pushing the amplitudes higher leads to saturation or nonlinear response. The same behaviour was observed for the transitional jet.

For brevity, here we only report the results of the jet with turbulent boundary layer forced at $St_f = 0.4$. Based on the response curves such as those of Figure 2, two forcing amplitudes were selected for further investigation with PIV measurements: one falling within the linear part and another well within the nonlinear response regime.

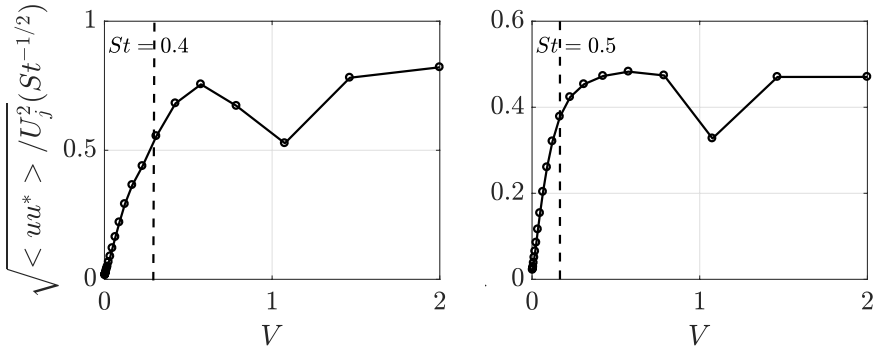

Fig. 2 Response of the turbulent jet to harmonic forcing at $St = 0.4, 0.5$. The three plots show the responses measured at each forcing frequency individually. Measurements were made at $x/D = 2$, $r/D = 0$. The vertical dashed lines approximately delimit the linear response regime.

IV. Tools

A. Spectral Proper Orthogonal Decomposition

We apply Spectral Proper Orthogonal Decomposition (SPOD) [12, 16] on the PIV database in order to study the spatial organisation of coherent structures and how they are modified in the different regimes of response to harmonic forcing. Given the state vector, $\mathbf{q} = [u, v]^T(x, y)$ obtained from the experiment, the SPOD modes for a given frequency ω_k, $\mathbf{\Psi}_{\omega_k}$ are obtained through the eigendecomposition of the cross-spectral density matrix, $\hat{\mathbf{S}}_{\omega_k}$,

$$\hat{\mathbf{S}}_{\omega_k}\mathbf{W}\mathbf{\Psi}_{\omega_k} = \mathbf{\Psi}_{\omega_k}\mathbf{\Lambda}_{\omega_k}. \tag{1}$$

The cross-spectral density matrix is computed as $\hat{\mathbf{S}}_{\omega_k} = \hat{\mathbf{Q}}_{\omega_k}\hat{\mathbf{Q}}^*_{\omega_k}$, where $\hat{\mathbf{Q}}_{\omega_k} = [\hat{\mathbf{q}}^{(1)}_{\omega_1}\hat{\mathbf{q}}^{(2)}_{\omega_1}\cdots\hat{\mathbf{q}}^{(N_{blk})}_{\omega_k}]$ is the ensemble of N_{blk} flow realisations at ω_k, with $\hat{\mathbf{q}}^{(l)}_{\omega_k}$ denoting the lth realisation of the Fourier transform in time at the $k$the frequency. The eigenvalues, $[\lambda^{(1)}_{\omega_k}, \lambda^{(2)}_{\omega_k}\cdots\lambda^{nblk}_{\omega_k}]$ corresponding to the modal energy are organised in decreasing order in the diagonal matrix $\mathbf{\Lambda}_{\omega_k}$. The modes so obtained are orthogonal in an inner product corresponding to the integral of squared velocity fluctuations on the PIV plane,

$$\langle \mathbf{q}_1, \mathbf{q}_2 \rangle = \iint \mathbf{q}_1^*\mathbf{q}_2 \mathrm{d}x\mathrm{d}r = \mathbf{q}_1^*\mathbf{W}\mathbf{q}_2; \tag{2}$$

where $\mathbf{W}$ is a weight matrix containing the numerical quadrature weights.

B. Bispectral mode decomposition

Bispectral mode decomposition is a novel technique [24] that has been developed in order to educe coherent structures associated with nonlinear triadic interactions. The main idea of the method consists in the maximization of an integral measure of the point-wise bispectrum (as opposed to SPOD, which seeks a maximization of the cross-spectrum) for a pair of frequencies f_k and f_l,

$$b(f_k, f_l) = E\left[\int_\Omega \hat{\mathbf{q}}_k^* \circ \hat{\mathbf{q}}_l^* \circ \hat{\mathbf{q}}_{k+l}^*\right] = E\left[\hat{\mathbf{q}}^H_{k\circ l}\mathbf{W}\hat{\mathbf{q}}_{k+l}\right] = E\left[\left\langle \hat{\mathbf{q}}^H_{k\circ l}, \hat{\mathbf{q}}_{k+l}\right\rangle\right], \tag{3}$$

where the inner product of the rightmost term takes the same definition as that used for SPOD. Here $\circ$ denotes a Hadamard product, and the compact notation

$$\hat{\mathbf{q}}_{k\circ l} \equiv \hat{\mathbf{q}}(\mathbf{x}, f_k) \circ \hat{\mathbf{q}}(\mathbf{x}, f_l) \tag{4}$$

denotes the point-wise product of two realizations of the flow at frequencies f_k and f_l. The method further defines two linear expansions,

$$\phi_{k\circ l}^{[i]} = \hat{\mathbf{Q}}_{k\circ l}\mathbf{a}_i, \tag{5}$$

$$\phi_{k+l}^{[i]} = \hat{\mathbf{Q}}_{k+l}\mathbf{a}_i, \tag{6}$$

with the same set of expansion coefficients, $\mathbf{a}$. $\hat{\mathbf{Q}}$ is the matrix containing the data blocks, as described above. These expansions allow the distinction between modes that are formed by the product of the interacting frequencies (cause), $\phi_{k\circ l}$, and modes that originate from that interaction (effect), following the triad

$$f_j \equiv f_k + f_l. \tag{7}$$

The latter are called bispectral modes, and can be thought of as observable flow structures.

The bispectrum mode decomposition then computes modes that optimally represent the data in terms of the global bispectrum, $b(f_k, f_l)$. This is achieved by seeking a set of expansion coefficients, $\mathbf{a}_1$ that maximize $b(f_k, f_l)$. Mathematically, this can be expressed as Rayleigh quotient

$$\mathbf{a}_1 = \arg\max \left| \frac{\mathbf{a}^H \mathbf{B}\mathbf{a}}{\mathbf{a}^H \mathbf{a}} \right|, \tag{8}$$

where $\mathbf{B}$ is the bispectral density matrix, given as,

$$\mathbf{B}(\mathbf{x}, f_k, f_l) \equiv \frac{1}{N_{blk}} \hat{\mathbf{Q}}_{k\circ l} \mathbf{W} \hat{\mathbf{Q}}_{k+l}. \tag{9}$$

This problem is solved by computing the numerical radius of $\mathbf{B}$, which is equivalent to the largest eigenvalue, λ_{max} that the Hermitian matrix

$$\mathbf{H}(\theta) = \frac{1}{2}\left(e^{i\theta}\mathbf{B} + e^{-i\theta}\mathbf{B}^H\right), \tag{10}$$

can attain for some angle $0 \leqslant \theta \leqslant 2\pi$. Then, the numerical radius is $\lambda_1 = \lambda_{max}\left(\mathbf{H}\left(\theta\right)\right)$ and the expansion coefficients, $\mathbf{a}_1$, maximize the Rayleigh coefficient 8. The reader is referred to Schmidt [24] for details about the numerical procedure. The maps of $\lambda_1(f_k, f_l)$ illustrate regions of the spectrum where there are significant quadratic phase-coupling between different frequencies, allowing the identification of three-wave interactions. In the framework of resolvent analysis, BMD can be interpreted as a maximization of the phase-alignment between a given quadratic, forcing term, $\hat{\mathbf{Q}}_{k\circ l}$, and an associated response, $\hat{\mathbf{Q}}_{k+l}$, respecting a given frequency triad.

V. Analysis

A. SPOD Eigenspectrum and coherent structures

Let us begin the analysis by identifying coherent structures present in the unforced jet through the SPOD modes (the eigenfunctions of $\hat{\mathbf{S}}_{\omega_k}$) and studying how their shapes and energy are modified by forcing at different amplitudes. Figure 3 shows the eigenvalue spectra of the SPOD for the forced and unforced jets. In the unforced case, the energy is seen to be mostly contained in the first two modes for a large portion of the spectrum covering $St \lesssim 0.8$. Beyond this frequency band, however, the energy is distributed much more equally among the modes, indicating that the flow does not exhibit any preference towards a physical mechanisms contained in a particular mode. As expected, the forcing produces an energy amplification at $St = 0.4$, as seen by the peaks at that frequency shown in 3(b) and 3(c). This amplification occurs, however, almost solely for the leading SPOD mode, whose associated physical mechanism then becomes dominant. The flow is then said to display low-rank behaviour [16]. At the lower level of forcing, amplification only occurs at the forcing frequency, demonstrating that the assumption of linear flow response is valid. At the higher forcing amplitude, on the other hand, energy is poured at other frequencies through nonlinear interactions. This is evidenced by the peaks at the harmonics of the forcing frequency which can be observed in 3(c). Unlike the energy increase at the harmonics, which are due to a purely nonlinear process, the enormous amplification at the forcing frequency $St_f = 0.4$ from the low-amplitude to the high-amplitude can be caused

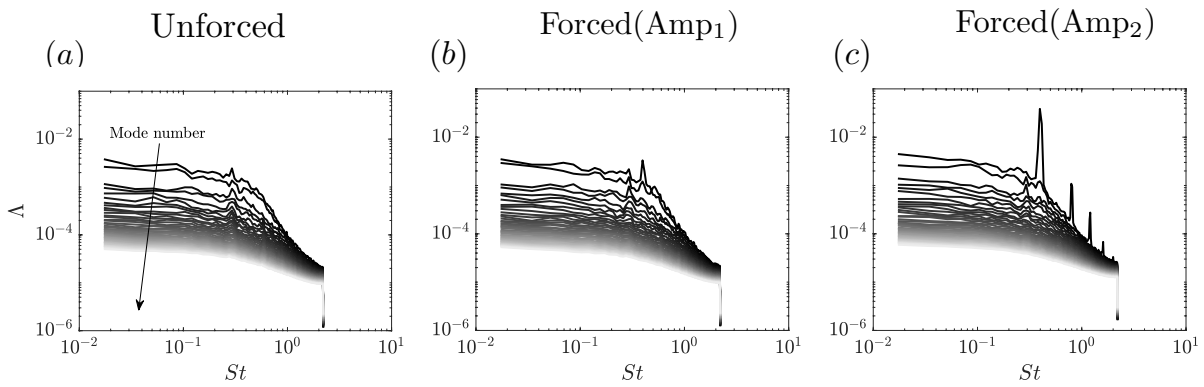

Fig. 3 Eigenvalue spectra of the SPOD. Color shading from black to white represent increasing mode numbers (, $\Lambda_1 > \Lambda_2 > ...\Lambda_N$). The forcing amplitude increase from left to right.

both by linear and nonlinear processes. Nevertheless, the relative importance of each to the global dynamics cannot be easily assessed through SPOD, which does not give any information about the flow of energy across different frequencies. This is analysed in more depth in section §V.B.

The spatial structures of the leading SPOD modes of forced and unforced jets are shown in Figure 4 for Strouhal numbers corresponding to the forcing frequency and its harmonics. At $St = 0.4$, the leading SPOD mode of the unforced jet exhibits the traits of coherent structures with large spatial lengthscales, which are commonly found in many shear flows. The periodic forcing reinforces the physical mechanism associated with those structures, enhancing their signature and spatial organisation and producing clear axisymmetric wavepackets. These are a typical feature of unforced turbulent jets [26, 27], but are made more easily detectable through the forcing. As mentioned in §II, it is this enhanced organisation that has motivated the use of harmonic forcing for coherent structure detection in early studies [1–4, 7–9, 18, 28–32].

At higher Strouhal numbers, $St = 0.8, 1.2, 1.6$, the SPOD modes of the unforced jet have spatial support in the shear-layer and exhibit decreasing levels of organisation as frequency is increased. The structure of these modes is not strongly altered with the low-amplitude forcing (except for some modification seen in 4(e)), but show considerable change with the high-amplitude forcing. Rather than highlighting the dynamics in the shear-layer, nonlinear interactions exploit a different mechanism, generating wavepackets in the core of the jet (Figure 4(f), 4(i), 4(l)). Such structures are generated by triadic interactions between the forcing frequency and its harmonics. In the next section, we identify the salient triadic interactions generated in the forced jets and we asses to what extent the BMD modes can reproduce the physical mechanisms of the most energetic structures revealed by SPOD.

B. BMD: linear and nonlinear mechanisms

The mode bispectrum reveals the regions of the spectrum where three-wave resonant interactions translate into high values of the numerical radius, $\lambda_1(f_k, f_l)$ of the bispectral matrix, $\mathbf{B}$ [24]. Figure 5 shows the mode bispectrum for forced and unforced jets. Due to its broadband energy content, the bispectrum of the unforced turbulent (5(a)) jet exhibits an extended signature of high nonlinear activity, which peaks roughly in the zone $St_k \lesssim 0.4$, $|St_l| \lesssim 0.3$. This signature is little affected by the low-amplitude forcing (5(b)), except for a local maximum generated at $(St_k, St_l) = (0.4, 0)$ confirming once again the hypothesis of linear response regime. With the high-amplitude forcing, on the other hand, a grid pattern is produced, featuring local maxima at the intersection of the forcing frequency and its harmonics. Figure 5(4) shows a zoom on the region of the grid pattern, where the most prominent triads are circled. The interaction of the fundamental forcing frequency with itself generates the first harmonic, $(f_k, f_l, f_k + f_l) = (0.4, 0.4, 0.8)$, which in turn interacts with the fundamental to generate the second harmonic, $(f_k, f_l, f_k + f_l) = (0.8, 0.4, 1.2)$, and so forth. It can also be seen that the self-interaction of the fundamental with its negative counterpart generates a maximum at the zero-frequency triad $(f_k, f_l, f_k + f_l) = (0.4, -0.4, 0)$, which accounts for the mean-flow distortion provoked by the high-amplitude forcing. A quantification of mean flow distortion and the bispectral modes that emerge

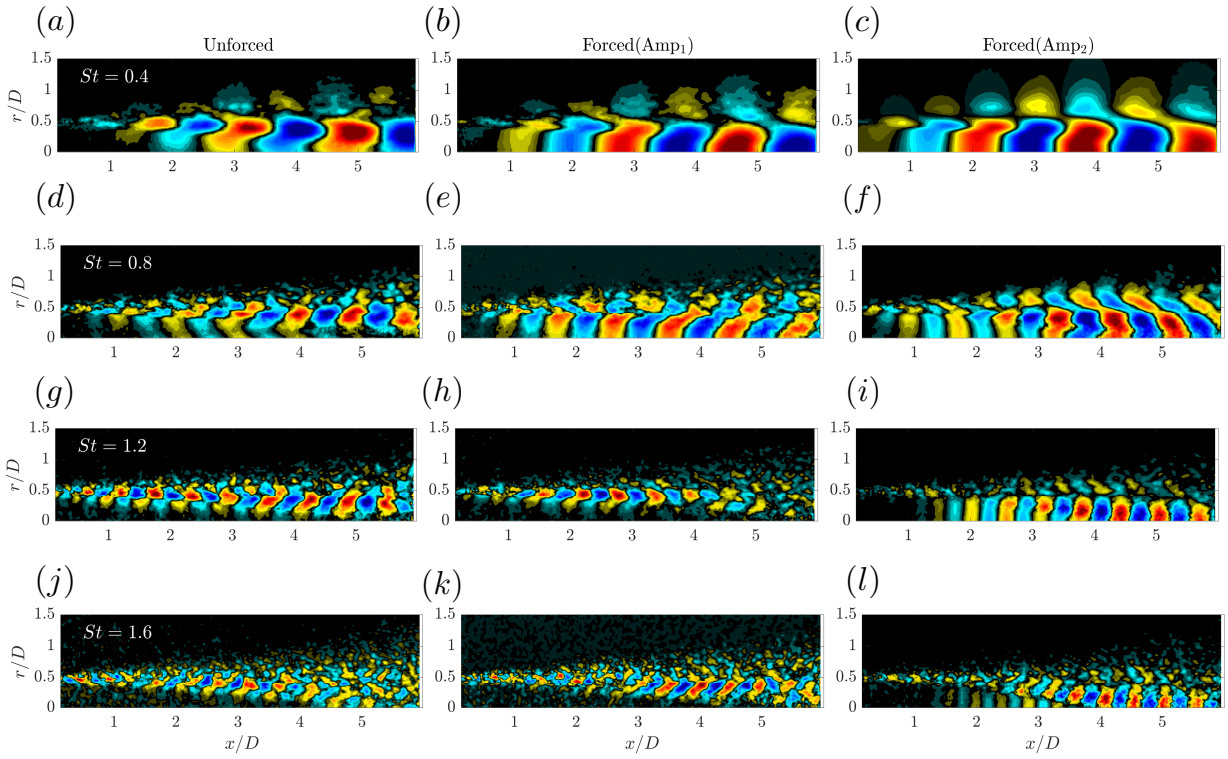

Fig. 4 Leading SPOD modes of the unforced and forced jets at Strouhal numbers corresponding to the forcing frequency and its harmonics: (a) $St = 0.4$; (b) $St = 0.8$; (c) $St = 1.2$; (d) $St = 1.6$. The streamwise velocity component, u, is shown. Contours are saturated at $\pm 90\%$ of the maximum values, for better visualisation.

from it are illustrated in Appendix §A.

The dashed line shown in 5(d) indicates a diagonal of constant frequency $St_{k+l} = St_f = 0.4$, i.e., it represents all the frequency triads that produce an effect at the forcing frequency. On this line, two local maxima stand out: one at $(f_k, f_l, f_k + f_l) = (0.4, 0, 0.4)$, which is reminiscent of a linear process (as are all points lying on the horizontal line sitting on the abscissa) of energy extraction from the mean flow, and one at$(f_k, f_l, f_k + f_l) = (0.8, -0.4, 0.4)$, which represents ta nonlinear exchange between the first harmonic on the fundamental. The relative magnitude of those two maxima gives us insight into the relative importance of linear and nonlinear amplification processes to the total energy of the velocity fluctuations at the forcing frequency, with respect to the mean flow of the forced jet. In order to quantify this more clearly, we show in Figure 6 the magnitude of the mode bispectrum along the diagonals ($St_k + St_l = St_f = 0.4$) for the forced and unforced cases. The linear triad $(0.4, 0, 0.4)$ is identified through vertical dashed lines. The magnitude of λ_1 decays exponentially with increasing St_k for the unforced jet. A slight peak exists at the linear triad, but its magnitude hardly stands out with respect to the other triads. This changes with the low-amplitude forcing, which greatly raises the amplitude of the linear piece, making it dominate the bispectrum at that frequency. A small peak can also be seen at the intersection of the fist harmonic with the fundamental, but its amplitude is five time smaller than that of the linear triad.

In the high-amplitude forced jet, the bispectrum is largely dominated by the $(St_k, (St_l, (St_{k+l}) = (0.4, 0, 0.4)$ and $(St_k, (St_l, (St_{k+l}) = (0.8, -0.4, 0.4)$ triads, which account for linear and nonlinear portions of the amplification of the velocity fluctuations at the forcing frequency, respectively. The nonlinear piece is predominant, but the linear part remains far from negligible, its magnitude being almost 70% that of the nonlinear triad.

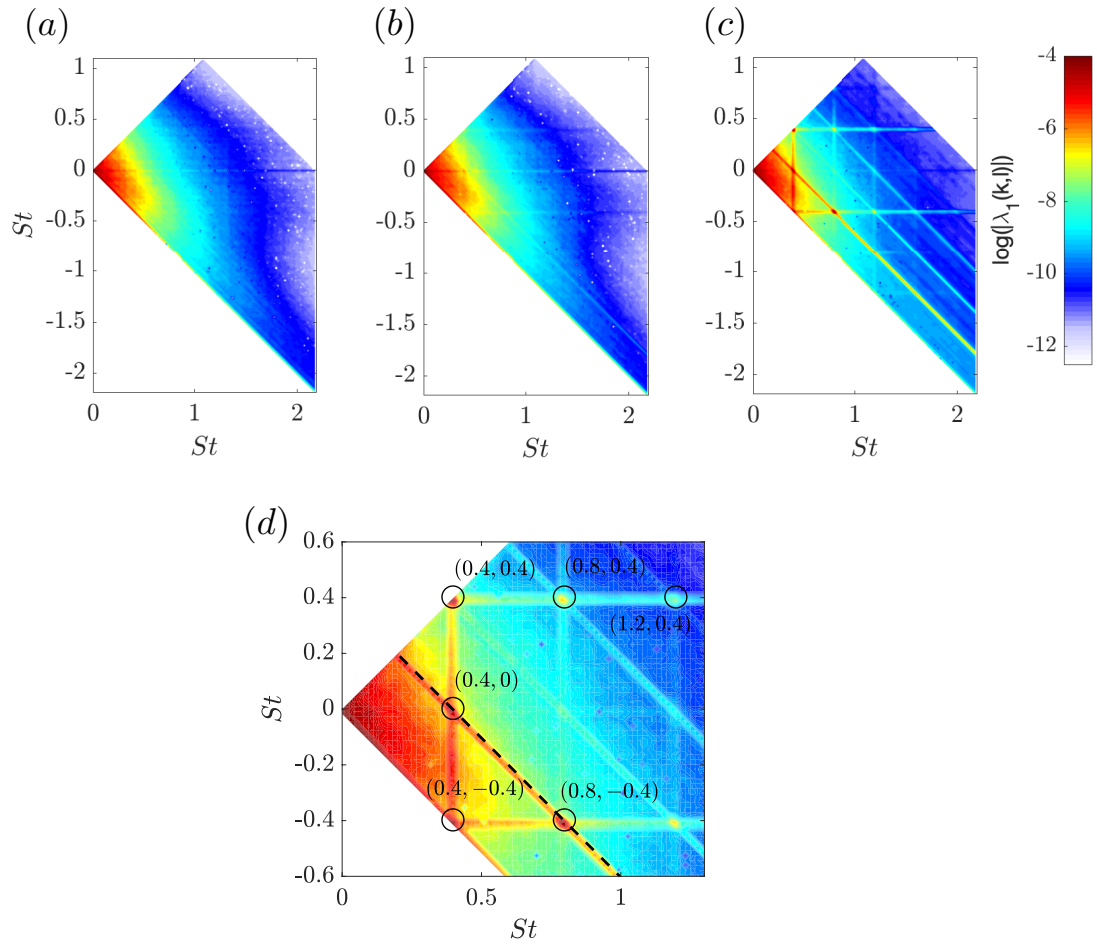

Fig. 5 Magnitude mode bispectra for the unforced jet (a) and the forced jets (b,c). Figure (d) shows a zoom around the region containing the most prominent triadic interactions. The dashed diagonal line represents constant frequency triads ($St_k + St_l = St_f = 0.4$)**.**

Bispectral modes issuing from triadic interactions that form at the harmonics of the forcing frequency are shown in Figure 7 for the strongly-forced jet. The modes correspond to the streamwise velocity component, ϕ^u_{k+l}. SPOD modes at frequency f_{k+l} are also shown for comparison. The SPOD and BDM modes are in excellent agreement, showing that BMD correctly computes the observed coherent structures associated with nonlinear interactions.

The associated cross-frequency fields, $\phi^u_{k\circ l}$ have a less clear physical interpretation, since they cannot be directly related to any flow structures. In the framework of resolvent analysis, where the equations of motion are separated into a linear left-hand side and an inhomogenous, nonlinear forcing term, these modes they can be thought of as the result of the projection of the forcing term on the forcing modes of the resolvent of the Navier-Stokes operator. For completeness, the cross-frequency fields of the triads shown in Figure 7 are depicted in Appendix §B.

C. Unforced jet: broadband nonlinear signature

In the forced jets, identification of the most important triads and associated BMD modes is straightforward due to the grid pattern generated by the relatively few interactions of the forcing frequencies with itself and its harmonics. The situation is less clear in the unforced jet, wherein its inherent broadband character does permit singling out one (or a few) dominant nonlinear mechanisms. Nevertheless, the mode bispectrum

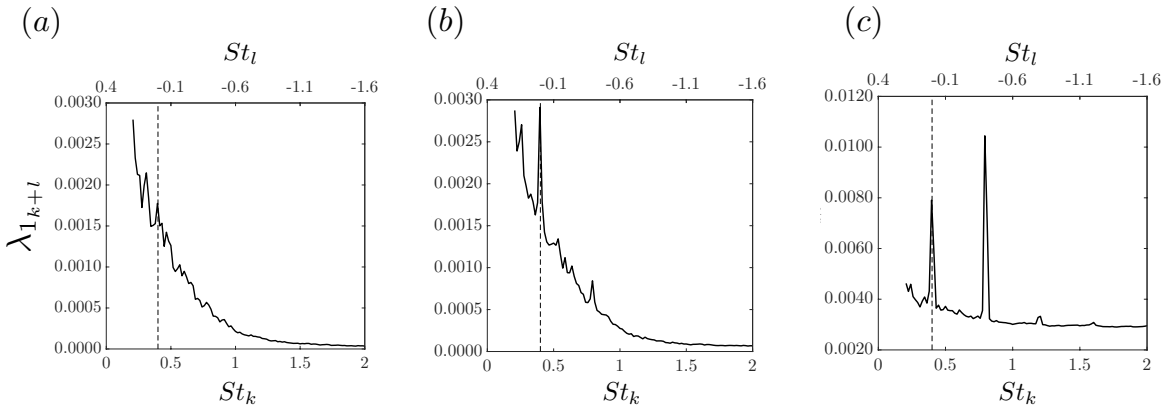

Fig. 6 Mode bispectrum along diagonal of constant frequency ($St_k + St_l = St_f = 0.4$). The bottom and top x-axes correspond to the $k-th$ and $l-th$ forcing frequencies, respectively. (a) Unforced jet; (b) low-amplitude forced jet; (c) high-amplitude forced jet. The vertical dashed line marks the triad $(0.4, 0, 0.4)$, representing a linear amplification mechanism.

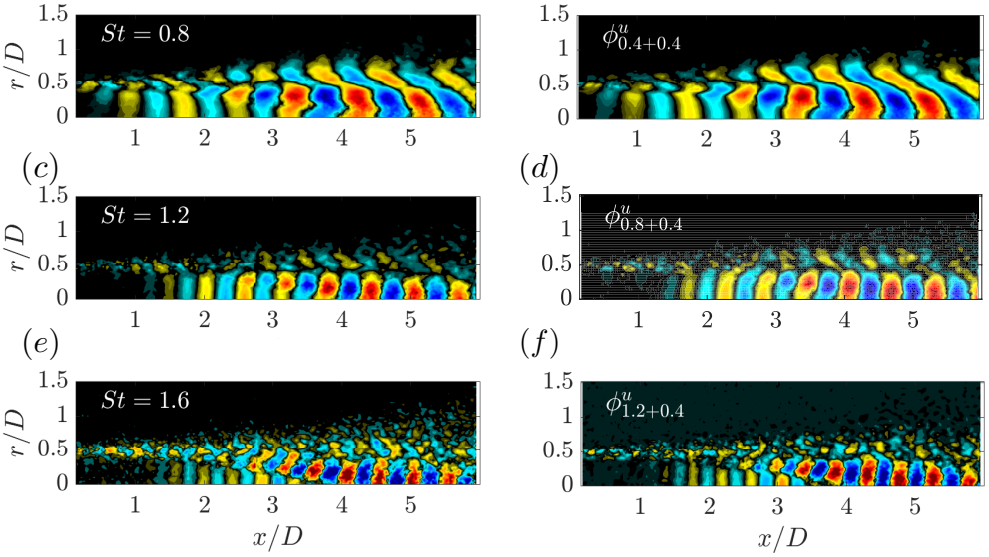

Fig. 7 Comparison between SPOD modes (a,c,e) and bispectrum modes issuing from individual triadic interactions. The streamwise velocity component, u, is shown. Contours are saturated for better visualisation.

shown in Figure 5(a) suggests that a stronger nonlinear coupling in the region $St_k \lesssim 0.4$, $|St_l| \lesssim 0.3$. This observation is consistent with previous studies [16, 17] which showed that both SPOD and resolvent analysis predict a zone of high-rank behaviour at $St < 0.3$. In this region, linear and/or modal instability mechanisms are not dominant (as opposed to the low-rank behaviour observed in the zone $0.3 \lesssim St \lesssim 2$), and modelling nonlinear mechanism becomes essential for an accurate representation of the salient flow dynamics.

It remains unclear, however, whether nonlinear effects are made stronger by the high energy of the flow structures involved at low frequencies (as evidenced by the SPOD eigenspectra of Figure 3, or by the intensity of the quadratic couplings themselves. In this sense, the bicoherence would provide a more precise metric than $\lambda_1(f_k, f_l)$ to measure the extent of deviation from linearity; but a normalisation of the bispectral matrix, $\mathbf{B}(\mathbf{x}, f_k, f_l)$ is not straightforward in the framework of BMD. Instead, in an effort to remove some of this ambiguity, we chose to normalise $\lambda_1(f_k, f_l)$ by the energy of the signal resulting from the phase-coupling,

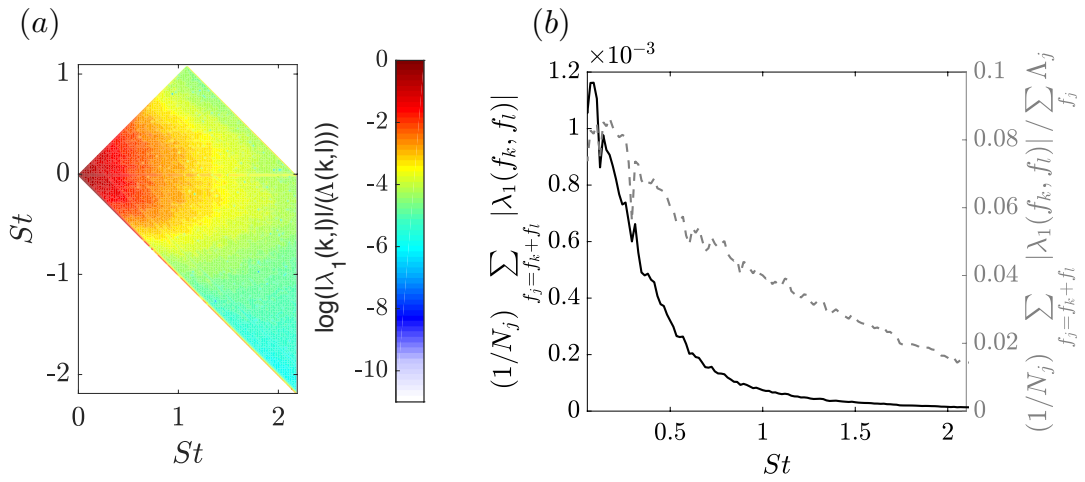

Fig. 8 Normalised mode bispectrum (a) and normalised summed mode bispectrum (b) for the unforced jet. Comparison with Figure 5(a) shows that normalising by the energy of the $j-th$ frequency in the triad $f_j \equiv f_k + f_l$ flattens the bispectrum. The non-normalised summed bispectrum (black solid curve) is also shown in (b) for comparison.

which we compute as the sum of the SPOD eigenvalues at the $j-th$ frequency of a given triad, $\sum_{f_j=f_k+f_l} \Lambda_j$. We also computed a normalised version of the summed mode bispectrum, which gives a more compact representation of the mode bispectrum [24],

$$\Lambda_1(f_j) = \frac{1}{N_{f_j}} \sum_{f_j=f_k+f_l} |\lambda_1(f_k, f_l)| \,/\, \sum_{f_j} \Lambda_j, \tag{11}$$

where N_{f_j} is the number of frequency doublets (f_k, f_l) that contribute to a given frequency $f_j = f_k + f_l$. Figure 8 depicts normalised mode and summed mode bispectra for the unforced jet. Comparison with the non-normalised version of Figure 5(a) reveals that normalising by the energy considerably flattens the bispectrum. The largest magnitudes are still found at lower frequencies, but the level of nonlinear activity remains important with increasing St, in spite of the decreasing energy of the flow mechanisms involved. This is something that should be kept in mind in future resolvent-based modelling studies.

VI. Concluding remarks

In this work we studied linear and nonlinear aspects of jet dynamics under varying degrees of external harmonic forcing. Special attention is given to nonlinear phenomena, analysed through the Bispectral Mode Decomposition technique. Working with forced jets can be considered as a first approach towards understanding and modelling nonlinear interactions in unforced jets, insofar as the most energetic flow structures issue from a reduced number of triadic interactions. These are identified through the mode bispectrum and correspond to the interactions of the forcing frequency with itself and its harmonics. The most energetic flow structures at the harmonics are computed through SPOD and are found to be in good agreement with the bispectral modes. This allows the nonlinear interactions responsible for the most energetic structures to be identified. By analysing the mode bispectrum along the diagonal line corresponding to the forcing frequency, one can assess the relative importance, with respect to the mean of the forced jet, of i) linear mechanisms of energy extraction from the mean and ii) nonlinear-exchange mechanisms across different frequencies. The two mechanisms contribute in determining the amplitude of the most energetic coherent structures. The unforced jet presents a much more challenging scenario for analysis and modelling, due to its broadband energy content. High nonlinear activity is found in an extended zone of the bispectrum, and it remains important even when the energy of the associated flow mechanisms is relatively small.

Future work will be focused on modelling of the nonlinear coherent structures revealed by SPOD and

BMD using resolvent analysis. The resolvent framework will also allow a physical interpretation of the cross-frequency BMD modes, which can be thought of as a quadratic forcing term.

A. Appendix: Mean flow distortion

Figure 9 addresses some features of mean flow distortion with the high-amplitude forcing. Mean flow contours for the unforced and forced jets are depicted in (a) and (b), respectively. It can be seen that the forcing shortens the potential core by more than one jet diameter. This is accompanied by thickening of the shear-layer, as evidenced is (c), which shows the streamwise evolution of the momentum thickness,

$$\theta = \int_0^\infty \frac{U(r)}{U_{r=0}} \left(1 - \frac{U(r)}{U_{r=0}}\right) \mathrm{d}r. \tag{12}$$

where U is the mean streamwise velocity. 9(d) and (e) show the bispectral and cross-frequency modes associated with the zero-frequency triad $(St_k, St_l, St_{k+l}) = (0.4, -0.4, 0)$ that produces the deformation. The bispectral mode is found to have spatial support in the shear-layer from about 1D, position at which the thickening of the shear-layer starts to occur. It then spreads across the radial direction and towards the jet axis as it develops downstream, following the shortening of the potential core.

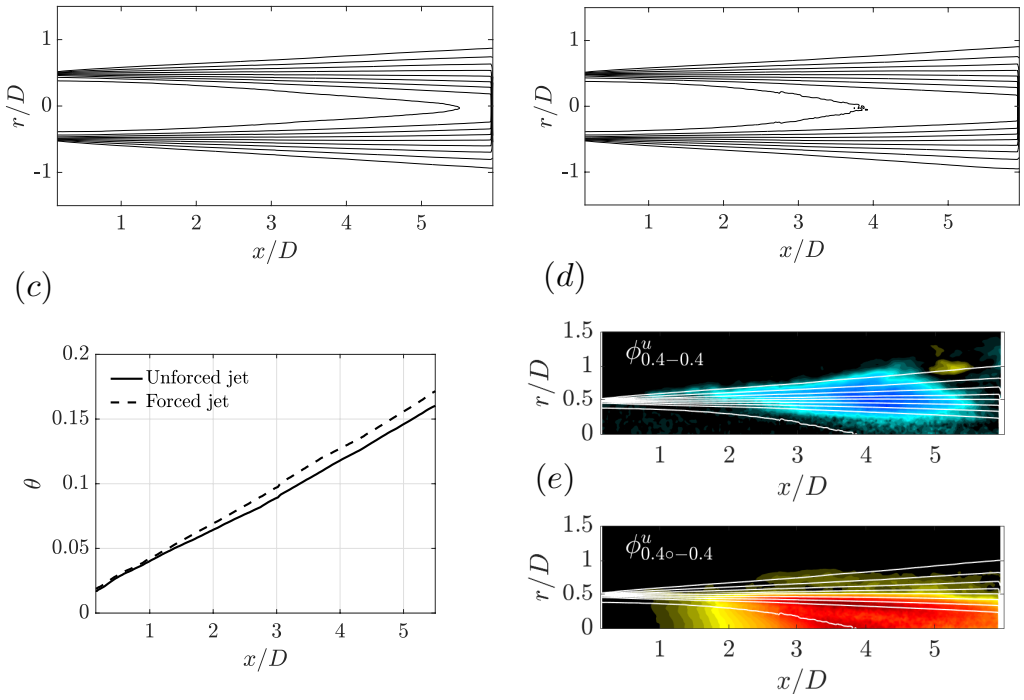

Fig. 9 Mean flow deformation with generated by the zero-frequency triad circled in Figure 5(d). (a) and (b) show mean flow contours of the unforced and forced jets, respectively. Contours are equally distributed between $U/U_j = 0.15$ and $U/U_j = 0.95$. (c): Streamwise evolution of the momentum thickness.(d) Bispectral mode issuing from the interaction of the forcing frequency, $St = 0.4$ with itself. (e): Cross-frequency modes for the same triad. Mean flow contours of the forced jet are superimposed in (d) and (e).

B. Appendix: Cross-frequency fields

Figure 10 shows the cross-frequency modes, ϕ^u_{kol}, of the triads circled in Figure 5(d) that correspond to harmonics of the forcing frequency, $St_f = 0.4$. Spatial support reveals a similar kind of core structure, as seen in ghe bispectral modes 7. However, physical interpretation of these modes is not entirely clear, as we cannot

assign them to an observable flow structure. In the framework of resolvent analysis, they can be understood as the projection of the inhomogeneous forcing term on the forcing modes of the resolvent operator. Previous studies [16, 17] have shown optimal forcing modes for turbulent jets to be concentrated around the jet lipline, exploiting and Orr-like mechanism, and subsequent suboptimal modes to be spatially extended. The spatial extent of the cross-frequency modes suggest the exploitation of multiple forcing mechanisms. But in the absence of resolvent analysis with the current database, this point remains, for the moment, speculative. This issue will be addressed in future modelling work.

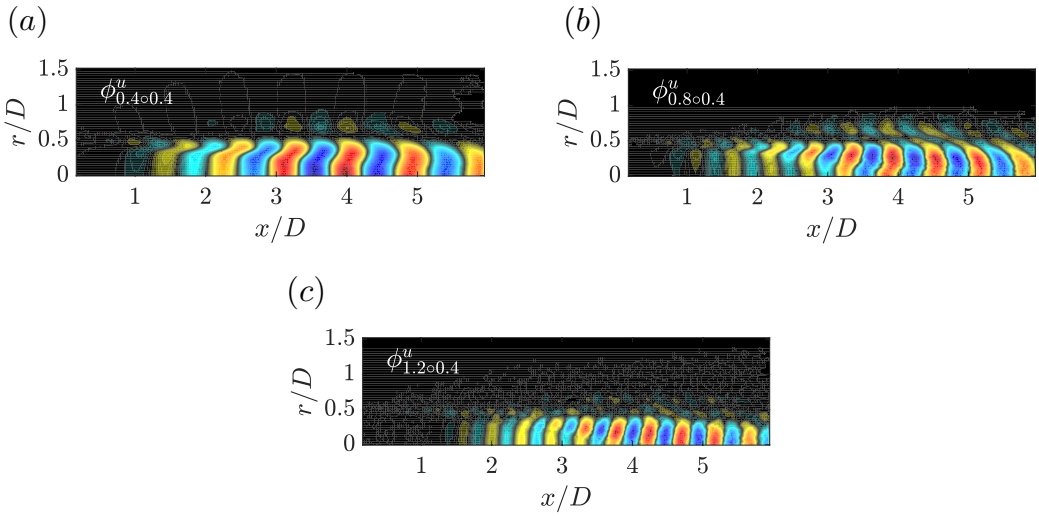

Fig. 10 Cross-frequency modes corresponding to the triads $(St_k, St_l, St_{k+l}) = (0.4, 0.4, 0.8)$, $(St_k, St_l, St_{k+l}) = (0.8, 0.4, 1.2)$, $(St_k, St_l, St_{k+l}) = (1.2, 0.4, 1.6)$ (circled in the bispectrum of Figure 5(d))and which are responsible for the nonlinear energy amplification at the harmonics of the forcing frequency. The streamwise velocity component is shown.

References

[1] Crow, S., and Champagne, F., "Orderly structure in jet turbulence," *Journal of Fluid Mechanics*, Vol. 48, 1971, pp. 547–591.

[2] Moore, C. J., "The role of shear-layer instability waves in jet exhaust noise," *Journal of Fluid Mechanics*, Vol. 80, 1977, pp. 321–367.

[3] Hussain, A. K. M. F., and Zaman, K. B. M. Q., "Vortex pairing in a circular jet under controlled excitation. Part 1: general jet response," *Journal of Fluid Mechanics*, Vol. 101, 1980, pp. 449–491.

[4] Hussain, A. K. M. F., and Zaman, K. B. M. Q., "Vortex pairing in a circular jet under controlled excitation. Part 2: coherent structure dynamics," *Journal of Fluid Mechanics*, Vol. 101, 1980, pp. 493–544.

[5] Hussain, A. K. M. F., and Zaman, K. B. M. Q., "The 'preferred' mode of the axisymmetric jet." *Journal of Fluid Mechanics*, Vol. 110, 1981, pp. 39–71.

[6] Petersen, R. A., and Samet, M. M., "On the preferred mode of jet instability," *Journal of Fluid Mechanics*, Vol. 194, 19988, pp. 153–173.

[7] Laufer, J., and Yen, T.-C., "Noise generation by a low-Mach-number jet," *Journal of Fluid Mechanics*, Vol. 134, 1983, pp. 1–31.

[8] Morrison, G. L., and McLaughlin, D. K., "Noise generation by instabilities in low Reynolds number supersonic flows," *Journal of Sound and Vibration*, Vol. 65, No. 2, 1979, pp. 177–191.

[9] Kibens, V., "On the role of vortex pairing in jet noise generation," *Proceedings of the Joint Symposium, Goettingen, West Germany, August 28-31, 1979. (A80-23890 08-71) Berlin, Springer-Verlag*, 1979, pp. 174–180.

[10] Cavalieri, A. V. G., Rodríguez, D., Jordan, P., Colonius, T., and Gervais, Y., "Wavepackets in the velocity field of turbulent jets," *Journal of fluid mechanics*, Vol. 730, 2013, pp. 559–592.

[11] Jaunet, V., Jordan, P., and Cavalieri, A. V. G., "Two-point coherence of wavepackets in turbulent jets," *Physical Review Fluids*, Vol. 2, No. 024604, 2017.

[12] Towne, A., Schmidt, O., and Colonius, T., "Spectral proper orthogonal decomposition and its relationship to dynamic mode decomposition and resolvent analysis," *Journal of Fluid Mechanics*, Vol. 847, 2018, p. 821–867.

[13] Gudmundsson, K., and Colonius, T., "Instability wave models for the near-field fluctuations of turbulent jets," *Journal of Fluid Mechanics*, Vol. 689, 2011, pp. 97–128.

[14] Sinha, A., Rodríguez, D., Brès, G., and Colonius, T., "Wavepacket models for supersonic jet noise," *Journal of Fluid Mechanics*, Vol. 742, 2014, pp. 71–95.

[15] Jeun, J., Nichols, J. W., and Jovanovic, M. R., "Input-output analysis of high-speed axisymmetric isothermal jet noise," *Physics of Fluids (1994-present)*, Vol. 28(4), No. 047101, 2016.

[16] Schmidt, O. T., Towne, A., Rigas, G., Colonius, T., and Brès, G. A., "Spectral analysis of jet turbulence," *Journal of Fluid Mechanics*, Vol. 855, 2018, pp. 953–982.

[17] Lesshafft, L., Semeraro, O., Jaunet, V., Cavalieri, A. V. G., and Jordan, P., "Resolvent-based modeling of coherent wave packets in a turbulent jet," *Physical Review Fluids*, Vol. 4, No. 063901, 2019.

[18] Zaman, K. B. M. Q., and Hussain, A. K. M. F., "Turbulence suppression in free shear flows by controlled excitation," *Journal of Fluid Mechanics*, Vol. 103, 1981, pp. 133–159.

[19] Bechert, D., and Pfizenmaier, E., "On the amplification of broadband jet noise by a pure tone excitation," *Journal of Sound and Vibration*, Vol. 43, 1975, pp. 581–587.

[20] Crighton, D. G., "Acoustics as a branch of fluid mechanics," *Journal of Fluid Mechanics*, Vol. 106, 1981, pp. 261–298.

[21] Raman, G., and Rice, E. J., "Axisymmetric jet forced by fundamental and subharmonic tones," *AIAA journal*, Vol. 29, 1991, pp. 1114–1122.

[22] Boze, G., and Hussain, F., "Nonlinear dynamics of forced transitional jets: periodic and chaotic attractors," *Journal of Fluid Mechanics*, Vol. 263, 1994, pp. 93–132.

[23] Shaabani-Ardali, L., Sipp, D., and Lesshafft, L., "Vortex pairing in jets as a global Floquet instability: modal and transient dynamics," *Journal of Fluid Mechanics*, Vol. 862, 2019, pp. 951–989.

[24] Schmidt, O. T., "Bispectral mode decomposition of nonlinear flows," *Nonlinear dynamics*, Vol. 102, 2020, pp. 2479–2501.

[25] Maia, I. A., Jordan, P., Cavalieri, A. V. G., Martini, E., and Silvestre, F., "Closed-loop control of forced turbulent jets," *arXiv preprint arXiv:2009.09299*, 2020.

[26] Jordan, P., and Colonius, T., "Wave Packets and Turbulent Jet Noise," *Annual Review of Fluid Mechanics*, Vol. 45, 2013, pp. 173–195.

[27] Cavalieri, A. V. G., Jordan, P., and Lesshafft, L., "Wave-packet models for jet dynamics and sound radiation," *Applied Mechanics Reviews*, Vol. 71, No. 020802, 2019.

[28] Favre-Marinet, M., and Binder, G., "Structure of pulsating jets," *Journal de Mécanique*, Vol. 18, No. 2, 1979, pp. 355–394.

[29] Jubelin, B., "New experimental studies on jet noise amplification," *6th Aeroacoustics Conference*, 1980.

[30] Ho, C. M., and Huerre, P., "Perturbed free shear-layers," *Annual Review of Fluid Mechanics*, Vol. 16, 1984, pp. 365–424.

[31] Raghu, S., Lehman, B., and Monkewitz, P., "On the mechanism of side-jet generation in periodically excited axisymmetric jets," *Advances in Turbulence 3: Proceedings of the Third European Turbulence Conference Stockholm*, 1990.

[32] Petersen, R. A., and Long, T. A., "Controlled interactions in a forced axisymmetric jet. Part 2. The modulation of broadband turbulence," *Journal of Fluid Mechanics*, Vol. 235, 1991, pp. 57–72.